9th ANKARA INTERNATIONAL AEROSPACE CONFERENCE AIAC-2017-198
20-22 September 2017 - METU, Ankara TURKEY

VALIDATION AND BENCHMARKING OF COMSOL 2D AXISYMMETRIC INDUCTIVELY COUPLED ARGON PLASMA MODEL

Erdal Bozkurt[1] and Ümmügül Erözbek Güngör[2]
Middle East Technical University
Ankara, TURKEY

Nafiz Alemdaroğlu[3]
Atılım Üniversitesi
Ankara, TURKEY

ABSTRACT

The numerical simulations of low-pressure radio-frequency (RF) inductively coupled argon discharge are carried out by using the finite element method (FEM) based on COMSOL Multiphysics® software program. Two-dimensional axisymmetric ICP model is used to compute the axial and the radial profiles of the electron density (n_e), the electron temperature (T_e) and the plasma potential (V_p). The axial analyses are obtained at two different gas pressures 30 and 40 mTorr for a fixed r=10 cm and P=300 Watt. While the radial measurements are done at P= 200, 300 and 400 Watt for a fixed z=4 cm and p=30 mTorr.

INTRODUCTION

The radio-frequency (RF) discharges (capacitive, inductive, microwave) are very popular in many industrial areas. Different modes are preferred for different industrial applications. The capacitive coupled cold plasmas are commonly used in microelectronics, surface modification, semiconductor processing (etching, deposition, sputtering) while the low-pressure (0.13 Pa to 1333 Pa [Lymberopoulos and Economou, 1995]), high-density (>10^{17} m^{-3} [Lymberopoulos and Economou, 1995]) inductively coupled plasmas are mostly used for in-space propulsion applications (ion thrusters).

The RF ion thrusters are composed of three main parts; inductive plasma generator, ion accelerator grids and electron neutralizer cathode as seen from Figure 1. For plasma generation, a grounded torch is wrapped by N-turn coil, which one end is directly connected to a RF (13.56 MHz or its harmonics) power supply. This generator applies an oscillating current to the Tesla coils that are responsible for the magnetic field generation around the torch. This is resulted in Ohmic (inductive) heating due to interaction of the created species (electrons and cations) in the plasma. It is important to get this temperature under control. For this reason, a cooling mechanism is necessarily required. By the way, there is a connection between the torch and an ion accelerator with two (or more) grids. The first grid is generally called as screen grid that is responsible for the ion extraction. The other ones are used to accelerate ions out of

---

[1] M.S. Student in Aerospace Engineering Department, METU, Email: e169695@metu.edu.tr
[2] PhD in Physics Department, METU, Email: ummugul@metu.edu
[3] Prof, Civil Aviation High School, in Atılım University, Email: nafiz.alemdaroglu@atilim.edu.tr

the torch by means of the applied high voltage. Finally, the third part (hallow cathode) is used for neutralization of the accelerated ion beam [Goebel and Katz, 2008].

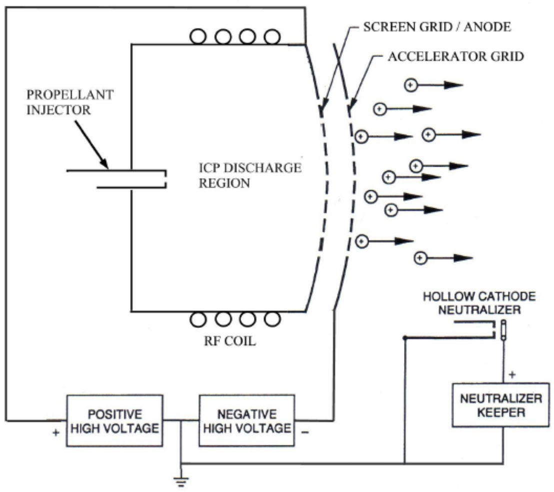

Figure 1. A typical schematic design of a RF-ICP ion thruster. [Tsay, 2010]

This paper presents validation and benchmarking of the self-consistent RF-ICP parametrical (electron density-n_e, electron temperature-T_e and plasma potential-V_p) simulations that are obtained via COMSOL Multiphysics software with an experiment [Gao, 2009]. The 2D axisymmetric FEM is used for numerical analysis according to the fluid dynamic assumption.

METHOD

The COMSOL Model

The computational analysis were run by using the frequency-domain ICP and Magnetic Field interfaces of COMSOL`s plasma and AC/DC modules, respectively. Two-dimensional (2D) axisymmetric finite element method (FEM) was used for numerical analysis. The simulation geometry of the our RF-ICP torch is clearly presented in Figure 2.

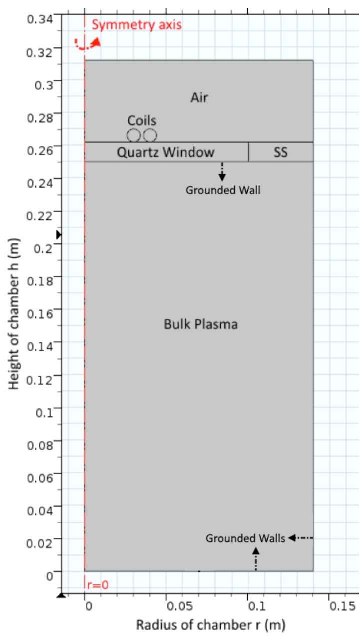

Figure 2. Simulation geometry of the RF-ICP torch

As seen from the Figure 2, two-turn coils (∅=0.95 cm) are placed onto a quartz window(ε_r=4.2, $\varnothing_{1/2}$=10 cm, $t_{thickness}$=1.2 cm). The coils are surrounded by an air medium for vacuum conditions. The symmetry axis is radial center of the RF-ICP torch (r=14 cm, h=25 cm). All torch walls are grounded (0 V). The computational domain is fulfilled with 36740 mesh elements and most of them are triangle in shape. The final mesh of the geometry and a closer view around the coils are shown in Figure 3.

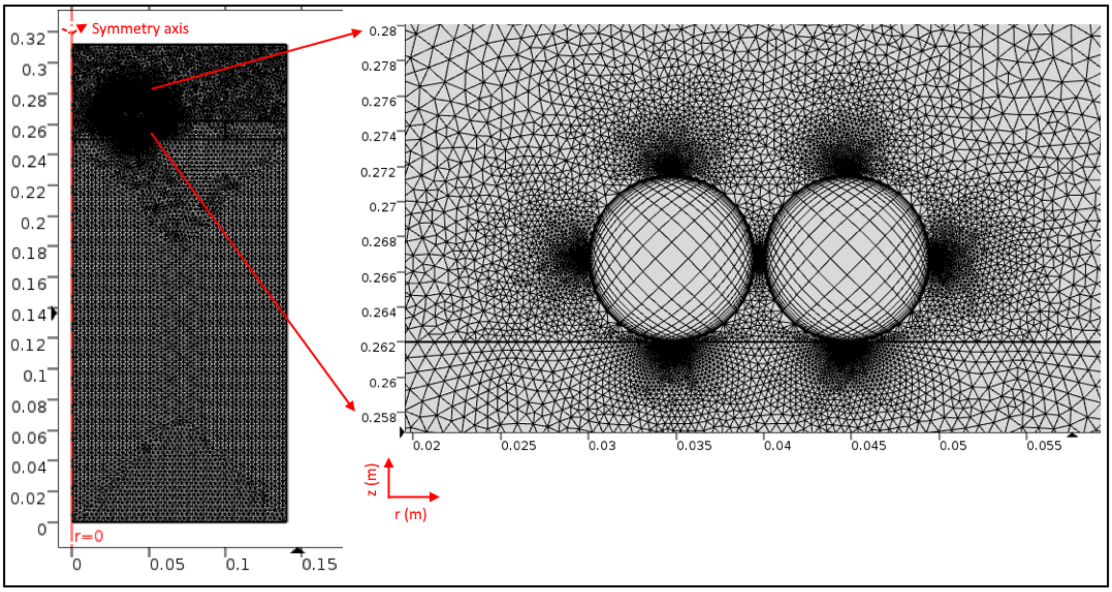

Figure 3. Mesh of the RF-ICP torch

The axial simulations (n_e, T_e and V_p) are run for pressures of 30 and 40 mTorr at fixed RF power of 300 Watt and radial distance of 10 cm whereas the radial ones are run for RF powers of 200, 300 and 400 Watt at fixed gas pressure of 30 mTorr and axial distance of 4 cm. The each simulation is completed in 6 minutes 40 seconds. The used processor is 4 GHz-AMD FX(tm)-8350 Eight-Core with 8 GB-RAM.

Theory

The fluid theory that is used to understand the physical mechanism of high-dense, continuum ICP (magnetized) plasmas is called as Magneto-hydrodynamics (MHD). In this theory, the Maxwell's equations are coupled with hydrodynamics. In fact, the origin of these equations is the Vlasov equations. The model equations are discretized with the finite element method (FEM). This numerical method is commonly used for solving the engineering, mathematical and physical problems. Some of the well-known physical problems are heat transfer, fluid flow, structural analysis, mass transport and electromagnetic problems.

Domain equations

The COMSOL ICP interface domain equations are mainly described by the Fluid (continuity or drift-diffusion equations) and the electromagnetic (Maxwell`s equations) submodels. In fact, there is a strong parametrical relation between these two submodels to get self-consistent solutions. As soon as getting values of electric and magnetic fields from the EM model, these values are used in the Fluid model to calculate plasma parameters. Then, the plasma conductivity is directly solved from these parameters and then it is inserted into the EM model. By this way, these two submodels are coupled to each other [Turkoz and Celik, 2015].

The fluid model states the average properties of the plasma particles by assuming the plasma is treated as a compressible gas. Another assumption is that all the plasma particles (the electrons, ions and neutrals) have a fluid dynamic.

The transport of electrons and the mean electron energy are described by the following drift-diffusion equations in 2D axisymmetric domain [Gao, 2009; Brezmes and Breitkopf, 2014 and 2015; Jia, 2013];

$$\frac{\partial n_e}{\partial t} + \nabla \cdot [-(\boldsymbol{\mu_e} \cdot \mathbf{E}) n_e - \mathbf{D_e} \cdot \nabla n_e] = R_e - (u \cdot \nabla) n_e \quad (1)$$

where n_e is the electron density, μ_e is the electron mobility, E is the electric field, D_e is the electron diffusivity, R_e is the electron source coefficient and $(u \cdot \nabla)n_e$ is the convective term (neglected for our calculations) [Gao, 2009; Brezmes and Breitkopf, 2014 and 2015; Jia, 2013];

$$\frac{\partial n_\varepsilon}{\partial t} + \nabla \cdot [-(\boldsymbol{\mu_\varepsilon} \cdot \mathbf{E}) n_\varepsilon - \mathbf{D_\varepsilon} \cdot \nabla n_\varepsilon] + \mathbf{E} \cdot \boldsymbol{\Gamma_e} = R_\varepsilon - (u \cdot \nabla) n_\varepsilon \quad (2)$$

where n_ε is the electrons energy, μ_ε is the electrons energy mobility, D_ε is the electrons energy diffusivity, $\mathbf{E} \cdot \boldsymbol{\Gamma_e}$ term is the joule (Ohmic) heating, R_ε is the gain or loss of electrons energy due to reactions and collisions and $(u \cdot \nabla)n_\varepsilon$ is the convective term (neglected for our calculations).

The steady-state electromagnetic fields inside the ICP reactor are calculated from the Maxwell`s equations by using the AC/DC module. For a known frequency, the induced currents are obtained by solving the following frequency domain Ampere`s law equation [Gao, 2009; Brezmes and Breitkopf, 2014 and 2015; Jia, 2013];

$$(j\omega\sigma - \omega^2 \varepsilon_0 \varepsilon_r)\mathbf{A} + \nabla \times (\mu_0^{-1} \mu_r^{-1} \nabla \times \mathbf{A}) = \mathbf{J_e} \quad (3)$$

where j is the imaginary part, ω is the angular frequency, σ is the plasma conductivity, ε_0 is the vacuum electric permittivity, ε_r is the relative electric permittivity, μ_0 is the magnetic vacuum permeability, μ_r is the relative magnetic permeability, A is the magnetic vector potential and J_e is the external current applied to the coil. For the electromagnetic model assumption, all the coils are connected in series and they have the same conduction current. In addition, the induced electric field and so the induced current is only in the azimuthal direction (no radial and vertical parts). Therefore, the input power can be written as [Gao, 2009; Brezmes and Breitkopf, 2014 and 2015; Jia, 2013];

$$P_{ind} = \frac{1}{2} \mathrm{real}(E_\emptyset \cdot J_{e\emptyset}) \quad (4)$$

where $E_\emptyset$ is the azimuthal component of the induced electric field, $J_{e\emptyset}$ is the azimuthal component of the induced current. Note that, the displacement current is neglected due to being very small as compared to the induced current.

Boundary and initial conditions

The number of electrons in the plasma decreases by loss due to reactor wall interaction but at the same time, it increases with the secondary electron generation in the plasma. Therefore, the general electron and energy flux equations can be written as [Brezmes and Breitkopf, 2015; COMSOL, 2013];

$$-\mathbf{n} \cdot \Gamma_e = \frac{1-r_e}{1+r_e}\left(\frac{1}{2} \nu_{e,th} n_e\right) - \left(\sum \gamma_i (\Gamma_i \cdot n) + \Gamma_t \cdot n\right) \quad (5)$$

$$-\mathbf{n}\cdot\Gamma_\varepsilon = \frac{1-r_e}{1+r_e}\left(\frac{5}{6}\nu_{e,th}n_\varepsilon\right) - \left(\sum\gamma_i\varepsilon_i(\Gamma_i\cdot n) + \varepsilon(\Gamma_t\cdot n)\right) \quad (6)$$

For our fluid model calculations, the boundary is the reactor wall. Therefore, we neglect the secondary emission flux terms ($\Sigma\gamma_i(\Gamma_i\cdot n)$ and $\Sigma\gamma_i\varepsilon_i(\Gamma_i\cdot n)$). In addition, we assume the thermal emission flux term ($\Gamma_t\cdot n$) is also zero. After setting the reflection coefficient (r_e) to 0.2, both boundary equations become [Brezmes and Breitkopf, 2015; COMSOL, 2013];

$$-\mathbf{n}\cdot\Gamma_e = \frac{1}{3}\nu_{e,th}n_e \quad \text{and} \quad -\mathbf{n}\cdot\Gamma_\varepsilon = \frac{5}{9}\nu_{e,th}n_\varepsilon \quad (7)$$

where **n** is the normal vector to the surface and $v_{e,th}$ is the electron thermal velocity.

Selection of initial conditions effects significantly verification of the used model. In any case, the first important initial condition is setting the voltage, V to “0” at t=0 to satisfy the Poisson equation. The second one is setting initial values of all magnetic vector potentials (axial, radial and azimuthal) as zero. For our calculations; driving RF frequency is 13.56 MHz, excitation inert gas is Argon, initial electron density ($n_{e,0}$) is 1×10^{15} m^{-3}, initial mean energy (ε_0) is uniform and equals to 5 V, initial reduced electron mobility (μ_{en}) is 4×10^{24} $m^{-1}V^{-1}s^{-1}$ and the gas temperature is 300 °K. In addition, the global coordinate system is used. The computational system reaches a steady state situation within 0.01 s.

Plasma chemistry

It is really hard to understand and explain the physical principles of inductively coupled plasma systems. Therefore, the simple and well-known Ar plasma chemical reaction mechanisms are preferred for this paper.

The Argon plasma is generated and sustained in an ICP torch. With the plasma ignition by RF generator in the torch, the electrons, radicals and ions are created with time. By this way, the plasma medium becomes conductive. The created species are mainly depend on RF frequency, gas flow and heating phenomena in the plasma. For our modeling, we only concentrated on the interaction between four species; e (electron), Ar (neutral), Ar^* (excited) and Ar^+ (singly-ionized) and their seven crucial chemical reaction processes are listed in Table 1 [Gao, 2009; Brezmes and Breitkopf, 2015; COMSOL, 2013];

Table 1. Modeled chemical reaction set in the ICP Argon discharge

No.	Process	Reaction	**Δε** (eV)
1	Elastic collision	$Ar + e \rightarrow Ar + e$	
2	Ground state excitation	$Ar + e \rightarrow Ar^* + e$	11.5
3	Ground state ionization	$Ar + e \rightarrow Ar^+ + 2e$	15.8
4	Step-Wise ionization	$Ar^* + e \rightarrow Ar^+ + 2e$	4.24
5	Superelastic collisions	$Ar^* + e \rightarrow Ar + e$	-11.5
6	Metastable pooling	$Ar^* + Ar^* \rightarrow Ar^+ + Ar + e$	
7	Two-Body quenching	$Ar + Ar^* \rightarrow Ar + Ar$	

Experimental setup

If any model code results are match up with the results of the experiment that is done under the same operating conditions, this model both verifies the theoretical assumptions and validates the experimental system. By this way, this model can be used for the further different related studies (RF-ICP ion thrusters). Therefore, in this section, we will mention about the appropriate experimental conditions to validate and benchmark our COMSOL ICP plasma module.

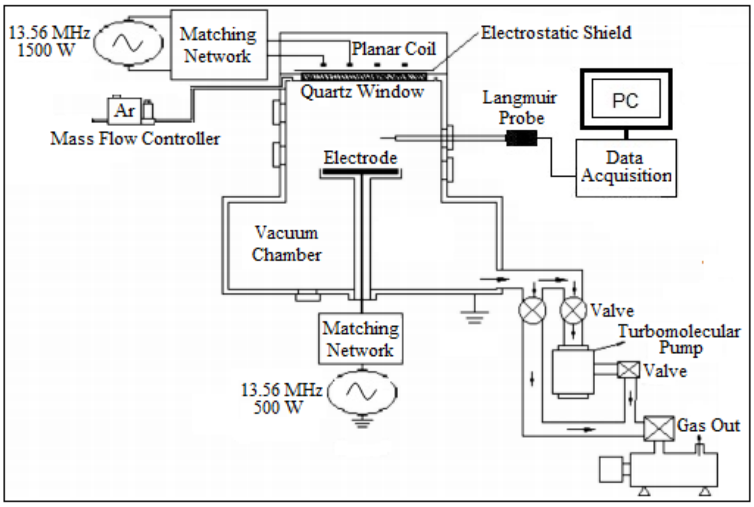

Figure 4. Schematic view of the planar-type ICP RF torch used for the experimental analysis [Gao, 2009]

A detailed sketch of the RF inductively coupled plasma torch is shown in Figure 4. As seen from the Figure 4, the shape of the torch seems like an inverse "T" letter. Therefore, we can separate geometry of the plasma torch into two parts; upper (I) and lower (−). The dimensions of the upper part are 28 cm in diameter and 25 cm in length. There is a quartz window (∅=20 cm and the thickness is 1.2 cm) on the top of the upper part. Two-turn planar coupling coil ($\varnothing_{outer}$=8 cm and $\varnothing_{inner}$=6 cm) that is put into a copper tube (for chilling) is attached to the outer surface of the quartz window. A 1500 W, 13.56 MHz RF source with its matching network system is connected to the coil. Volume (∅=30 cm, h=21 cm) of the lower part is a bit smaller than that of the upper part. A Teflon isolated aluminum electrode is welded to the bottom of the lower part. The electrode is connected to another grounded 500 W 13.56 MHz RF source to ignite the plasma. For diagnostic analysis, a commercial (Hiden Probe, Hiden Analytical, Ltd.) Langmuir probe is inserted into the torch at a 4 cm fixed distance away from the upper part for radial parametrical analysis and 10 cm fixed distance away from the central axis of the torch for axial analysis. The probe tip is a tungsten wire, which diameter is 0.2 mm and length is 10 mm. A mass flow controller unit controls the amount of the Argon gas in the plasma.

Results and Discussion

Figures 5-9 present the experimental and simulated axial distributions of RF-ICP plasma parameters (n_e, T_e and V_p) at 10 cm radial distance and 300 Watt RF coil power under two different (30 and 40 mTorr) gas pressures.

The axial electron density evolution is shown in Figure 5. The simulated results almost match up with the experimental results. A similar increase in the density is shown with the gas pressure in both cases due to high collision rate. According to the measured data, the electron density is nearly constant in the bulk plasma region at the torch center and it decreases toward to the sheath regions that are closer to the top and the bottom walls. On the other hand, the numerical results that are obtained in this limited (up to z=12 cm) region become constant. As soon as the simulations cover the whole z-domain as seen in Figure 6, the density decreases toward to the bottom sheath region. In fact, the main reason of this difference is using very low diffusion and drift electron velocities in the simulation results. In addition, from the Figure 6, both species have almost the same profile (quasi-neutrality) except towards the boundaries. The ion density on the right boundary (bottom of the chamber-cathode) is almost 10 times greater than the electron density because of the ion shielding while the electron density is 1.3 times greater than the ion density on the left boundary (quartz window-anode) due to the electron shielding.

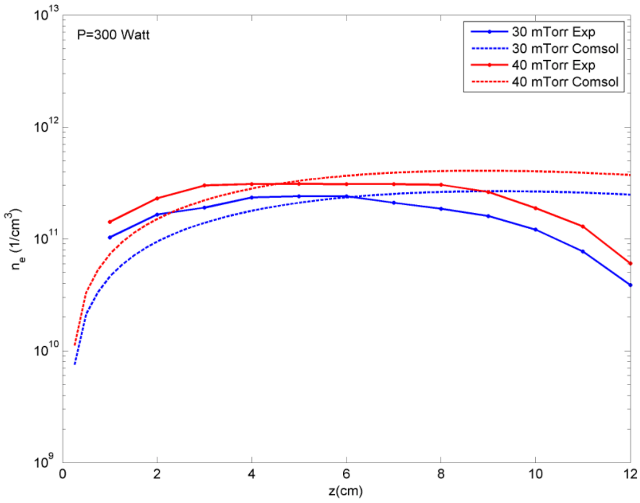

Figure 5. The axial distribution of the electron density for both simulated and experimental results operated for 30 and 40 mTorr at r=10 cm and P=300 Watt

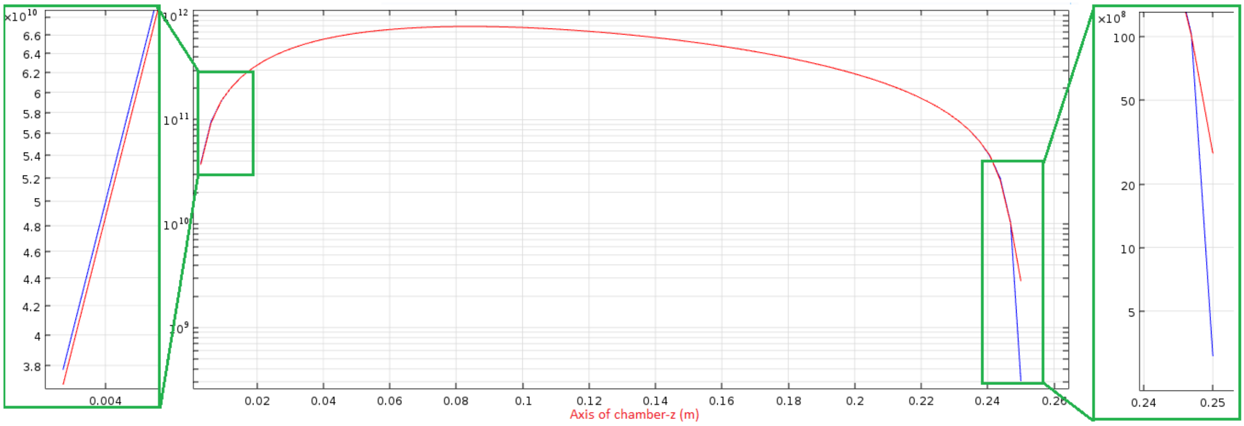

Figure 6. The extended axial distribution of n_e-blue line and n_i-red line for the simulated results operated for 30 mTorr at r=10 cm and P=300 Watt

Figure 7 shows the axial profiles of simulated and measured electron temperature of RF inductively coupled discharges under the same operating conditions (30 and 40 mTorr, 300 Watt). The values of the simulated temperatures are lower than that of the experimental results. The measured data reveals that the temperatures decrease gradually toward the sheath regions due to increasing azimuthal electric field (or induced power) and almost stable in the bulk plasma region where the E-field (or the power) is almost zero. Also, they decrease with the gas pressure except the edges of the dielectric walls. However, the simulated temperatures decrease along the axial distance. Although as if there is a large deviation between the experimental and the simulated results, the average difference is about 0.4 eV.

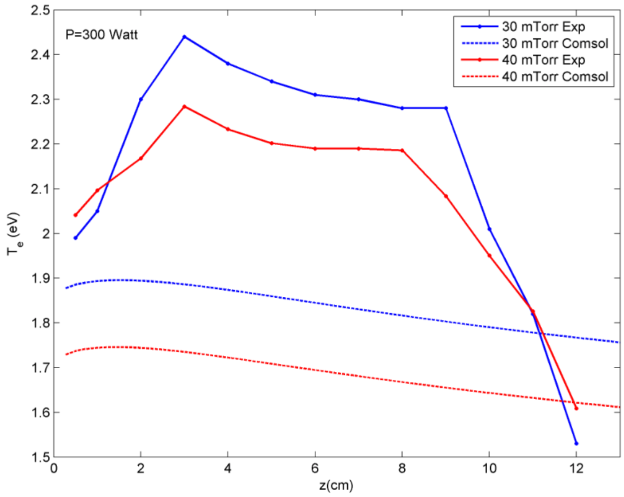

Figure 7. The axial distribution of the electron temperature for both simulated and experimental results operated for 30 and 40 mTorr at r=10 cm and P=300 Watt

The comparison of the plasma potential variation along the axial distance is shown in Figure 8. All the profiles are very similar to that of the electron density. However, the experimental potential values are higher than the calculated potentials. Almost none change is observed with the gas pressure. By covering the whole z-domain as seen in Figure 9, the simulated potential drops (0 V) in the sheath region is clearly observed. As mentioned before, the reason of these further drops is low diffusion and drift electron velocities in the simulated data. Moreover, the simulated results are almost 4 V lower than the measured values.

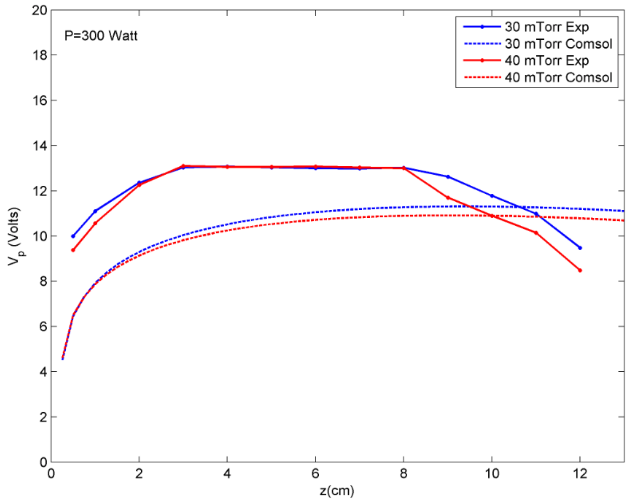

Figure 8. The axial distribution of the plasma potential for both simulated and experimental results operated for 30 and 40 mTorr at r=10 cm and P=300 Watt

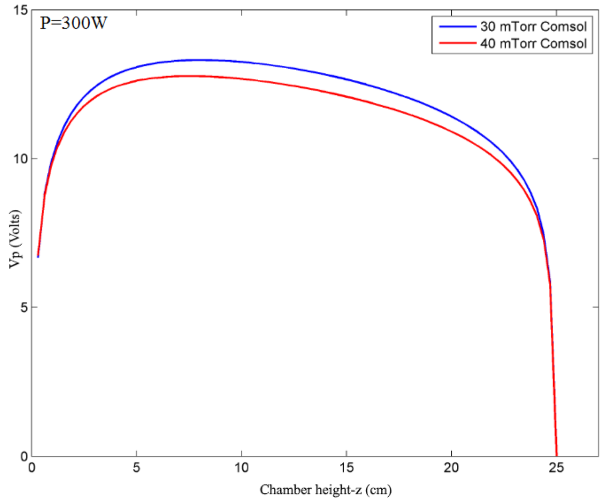

Figure 9. The extended axial distribution of the plasma potential of the simulated results operated for 30 and 40 mTorr at r=10 cm and P=300 Watt

The radial distribution of the plasma parameters (n_e, T_e and V_p) for three different RF powers; 200, 300 and 400 Watt at z=4 cm and 30 mTorr are presented in Figures 10-12. From the Figure 10, both calculated and measured electron density profiles decrease with the radial distance and they are almost the same except that of 200 Watt.

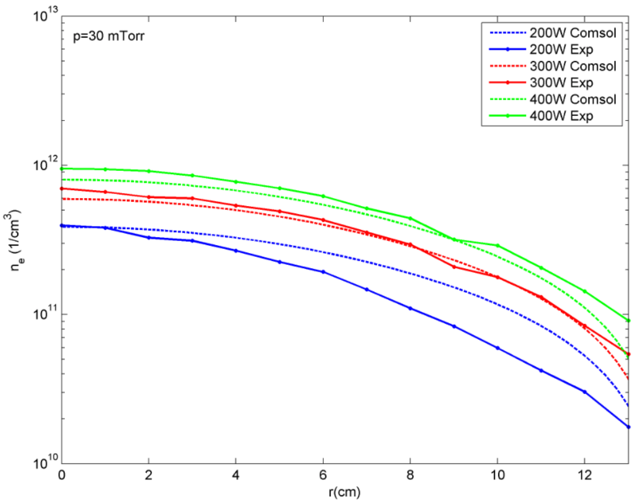

Figure 10. The radial distribution of the electron density for both simulated and experimental results operated for 200, 300 and 400 Watt at z=4 cm and p=30 mTorr

From the Figure 11, the numerical electron temperatures are lower than that of the experimental measurements. In fact, their radial profiles are almost similar. Both decreases with the radial distance and they get closer to each other toward the right wall of the torch. There is no RF power effect on the calculated electron temperatures whereas the temperature increases with the RF power according to the experimental results. There is an almost 1.2 eV difference between the numerical and the experimental values and it decreases gradually with the radial distance.

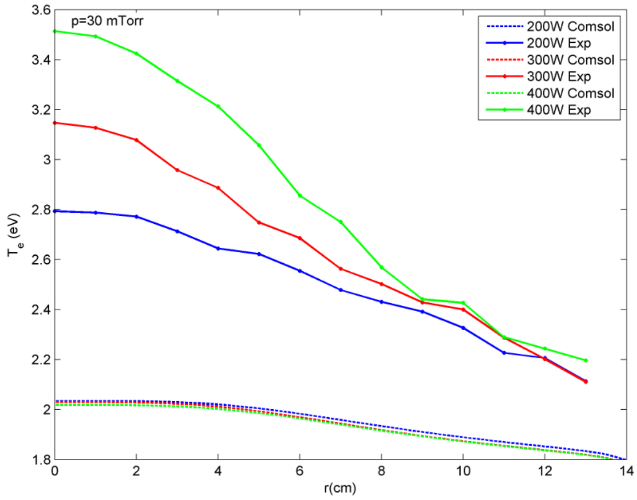

Figure 11. The radial distribution of the electron temperature for both simulated and experimental results operated for 200, 300 and 400 Watt at z=4 cm and p=30 mTorr

From Figure 12, both results have similar plasma potential profile curves for all RF powers under the same gas pressure (30 mTorr). As mentioned in the radial temperature analysis, no RF power effect is observed with the numerical results while a slight increase is clearly detected with increasing power. In both cases, the plasma potential decreases toward to the side walls. Also, the overall difference between the simulated and the measured results is approximately 4 V.

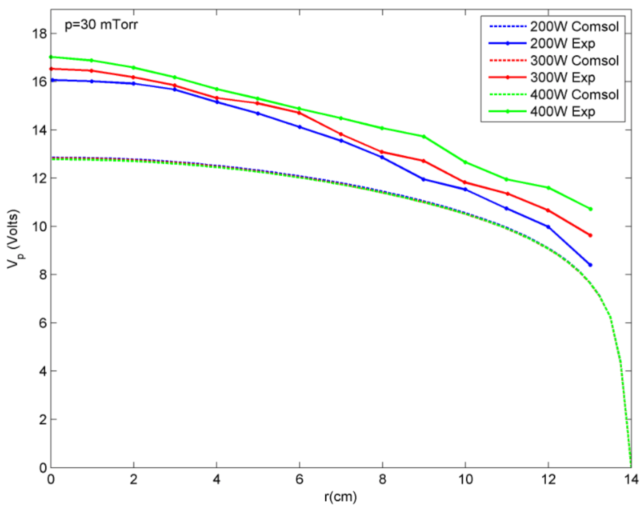

Figure 12. The radial distribution of the plasma potential for both simulated and experimental results operated for 200, 300 and 400 Watt at z=4 cm and p=30 mTorr

In conclusion, 2D axisymmetric fluid and global models are used for simulating the argon two-coil planar RF-ICP discharges by using the COMSOL software and the results are compared with that of experimental results. The axial and radial evolutions of the electron density, the electron temperature and the plasma potential are analyzed by both cases. The plasma operating conditions as compared to the simulated ones mostly affects the experimental results. However, in general, the model simulations match up with the measured results. Therefore, the next step is to develop used model for simulating a RF ion thruster.

References

Breitkopf C. and Brezmes A. O. (2015) *Fast and reliable simulations of argon inductively coupled plasma using COMSOL*, Vacuum, Vol. 116, p:65-72, 2015.

Breitkopf C. and Brezmes A. O. (2014) *Simulation of inductively coupled plasma with applied bias voltage using COMSOL*, Vacuum, Vol. 109, p:52-60, 2014.

Celik M. and Turkoz E. (2015) *AETHER: A simulation platform for inductively coupled plasma,* Journal of Computational Physics, Vol. 286, p:87-102, 2015.

Chuankun H., Jia C., Kesheng W., Linhong J. and Yixiang S. (2013) Two-dimensional simulation of inductively coupled plasma based on COMSOL and comparison with experimental data, Journal of Semiconductors, Vol. 34, June 2013.

COMSOL, *GEC ICP Reactor, Argon Chemistry*, COMSOL Multiphysics 4.3b Manual, 2013.

Economou D. J. and Lymberopoulos D. P. (1995) *Two-Dimensional Self-Consistent Radio Frequency Plasma Simulations Relevant to the Gaseous Electronics Conference RF Reference Cell,* J. Res. Natl. Inst. Stand. Technol., Vol. 100, July-August 1995.

Gao, F., Li X., Wang Y. and Zhao S., (2009) *Comparison between experiment and simulation for argon inductively coupled plasma,* Physics of Plasmas, Vol. 16, p:1-8, November 2009.

Goebel, D. M. and Katz, I. (2008) *Fundamental of Electric Propulsion: Ion and Hall Thrusters, March*, Wiley, ISBN: 978-0-470-42927-3, November 2008.

Tsay, M. M. (2010) *Two-Dimensional Numerical Modeling of Radio-Frequency Ion Engine Discharge*, Thesis, August 2010.

List of Figures

Figure 11. The radial distribution of the electron temperature for both simulated and experimental results operated for 200, 300 and 400 Watt at z=4 cm and p=30 mTorr

Figure 12. The radial distribution of the plasma potential for both simulated and experimental results operated for 200, 300 and 400 Watt at z=4 cm and p=30 mTorr